An approximation for NLO single Higgs boson inclusive transverse momentum distributions in hadron-hadron collisions

J. SMITH [1]

C.N. Yang Institute for Theoretical Physics,
State University of New York at Stony Brook, New York 11794-3840, USA.

W.L. VAN NEERVEN

Instituut-Lorentz
University of Leiden,
PO Box 9506, 2300 RA Leiden,
The Netherlands.

January 2005

Abstract

In the framework of the gluon-gluon fusion process for Higgs boson production there are two different prescriptions. They are given by the exact process where the gluons couple via top-quark loops to the Higgs boson and by the approximation where the top-quark mass m_t is taken to infinity. In the latter case the coupling of the gluons to the Higgs boson is described by an effective Lagrangian. Both prescriptions have been used for the $2 \to 2$ body reactions to make predictions for Higgs boson production at hadron colliders. In next-to-leading order only the effective Lagrangian approach has been used to compute the single particle inclusive distributions. The exact computation of the latter has not been done yet because the n-dimensional extensions of $2 \to 3$ processes are not calculated and the two-loop virtual corrections are still missing. To remedy this we replace wherever possible the Born cross sections in the asymptotic top-quark mass limit by their exact analogues. These cross sections appear in the soft and virtual gluon contributions to the next-to-leading order distributions. This approximation is inspired by the fact that soft-plus-virtual gluons constitute the bulk of the higher order correction. Deviations from the asymptotic top-quark mass limit are discussed.

PACS numbers: 1238.-t, 13.85.-t, 14.80.Bn.

---

1 Introduction

In the past few years many articles have appeared on searches for the Higgs boson and the reactions in which they are produced. One of them is the gluon-gluon fusion process. According to the standard model gluons do not interact directly with the Higgs boson but the coupling is mediated by a fermion loop. Since the coupling of the Higgs boson to fermions is proportional to the mass of the fermion the reaction proceeds mainly via a top-quark loop [1]. The lowest order loop is a triangle graph and the Higgs boson decay rates into two gluons or two photons were already calculated at the end of the seventies [2]. The first calculation in the gluon-gluon-fusion model for the production process was done at the end of the eighties by [3]-[5], (see [6],[7] for later references). Reactions like $g + g \rightarrow g + H$, $q + \bar{q} \rightarrow g + H$ and $q + g \rightarrow q + H$ were calculated. In particular the first reaction involves a box diagram leading to complicated dilogarithms already on the Born level. In the early nineties people succeeded in calculating the next-to-leading order (NLO) corrections to the total cross section which involved the computation of the two-loop triangular graph with an external Higgs boson [8]. The calculation could be greatly simplified by taking the infinite top-quark mass limit. In this limit the gluons couple directly to the Higgs boson and the Feynman rules are given by an effective Lagrangian. It turned out that the latter method gives a good description of the exact calculation [9] provided the Higgs boson mass m_H and the transverse momentum p_t are smaller than the top-quark mass m_t [4], [5], [7]. In particularly the total cross section receives its main contribution from small p_t. If the Higgs mass is not too large $(m_H < 2\,m_t)$ the effective Lagrangian gives a good description of the total cross section so that recently one has also finished the next-to-next-leading order (NNLO) computation [10]-[14]. However at Higgs masses and transverse momenta equal or larger than the top-quark mass the differential cross sections calculated with the effective Lagrangian method start to deviate from the exact cross sections. This has been checked on the Born level in [4], [5], [7]. The investigation should now be done in NLO but we realize that the exact cross sections are not available. Differential distributions in NLO using the effective Lagrangian (or the $m_t \rightarrow \infty$ approach) have been calculated in [15]-[18]. In the same approach the resummation of the logarithmically enhanced contributions to $d\sigma/dp_t$ at small p_t have been carried out in [19] -[21]. The first landmark calculation to get the full NLO differ-

ential distribution has been achieved in [22]. In the latter one has exactly calculated all matrix elements of the $2 \to 3$ processes. These reactions even contain one-loop five-point functions. However the calculation of the graphs uses the helicity method in four dimensions. To compute the single particle inclusive process we need the matrix elements in n dimensions. Moreover the two-loop virtual corrections, which are needed to cancel the infrared and collinear divergences, have not been calculated yet. Therefore we propose to make an approximation by replacing all Born contributions in the infinite top-quark mass limit by their exact analogues in the virtual-plus-soft corrections. However this is not sufficient. We have also to demonstrate that the soft-plus-virtual gluon approximation gives a good description of the differential cross section. Using a certain prescription we can show that this is really the case.

Our paper is organized as follows. In Section 2 we present the formulas for the exact cross sections and their analogues in the infinite top-quark mass limit. Then we make approximations for the partonic soft-plus-virtual and the soft-gluon cross sections. Finally we adopt a prescription how to implement these formulae for the hadronic p_t distributions. In Section 3 we make comparisons between our approximate differential distributions and those which are derived in the limit $m_t \to \infty$.

3

2 Approximation to the exact differential cross section for Higgs production

The differential process we study is the semi-inclusive reaction with one Higgs boson H in the final state

$$H_1(P_1) + H_2(P_2) \rightarrow H(q) +' X'. \qquad (2.1)$$

Here H_1 and H_2 denote the incoming hadrons and X represents an inclusive hadronic state. In our study we limit ourselves to $2 \rightarrow 2$ and $2 \rightarrow 3$ partonic subprocesses. The kinematics of the $2 \rightarrow 2$ reaction is
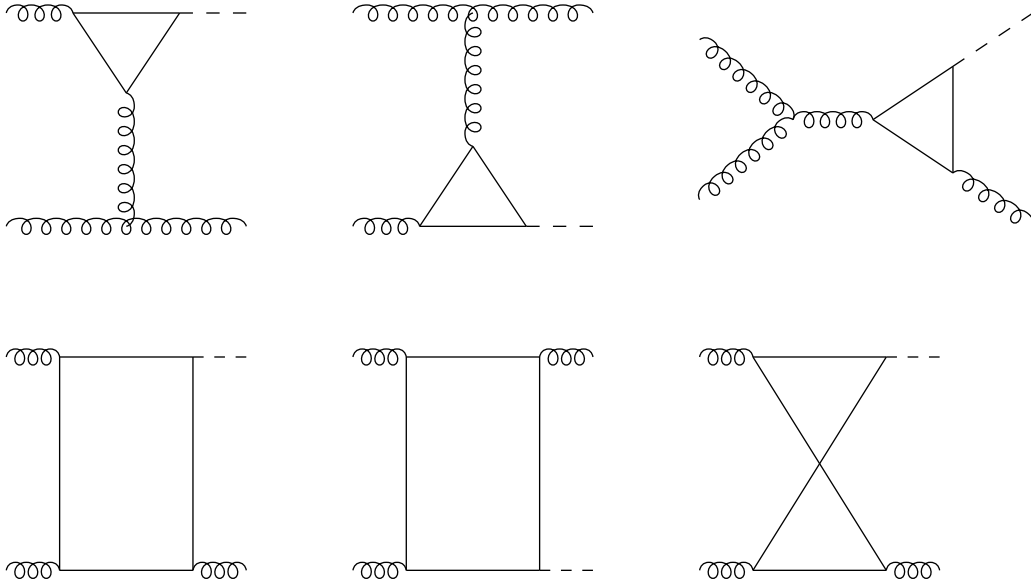

Figure 1: The exact process $g + g \rightarrow g + H$.

$$a(p_1) + b(p_2) \rightarrow c(p_3) + H(q),$$

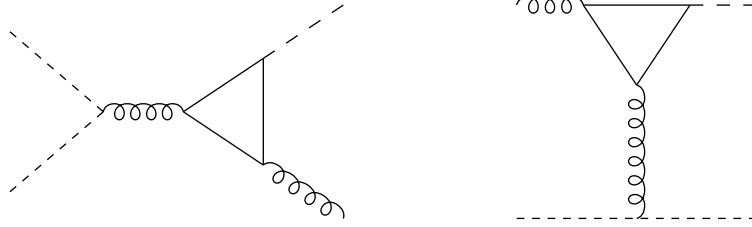$$s = (p_1 + p_2)^2, \qquad t = (p_1 - q)^2, \qquad u = (p_2 - q)^2. \qquad (2.2)$$

Figure 2: The exact processes $q + \bar{q} \to g + H$ and $q(\bar{q}) + g \to q(\bar{q}) + H$.

The exact calculations of the $2 \to 2$ processes are given in [3]-[7]. They consist of the following parton subprocesses

$$g + g \to g + H\,, \qquad q + \bar{q} \to g + H\,, \qquad q(\bar{q}) + g \to q(\bar{q}) + H\,. \qquad (2.3)$$

The Born cross section for the $g + g \to g + H$ subprocess in Fig. 1 is equal to

$$s^2 \frac{d^2 \sigma_{gg \to g\ H}^{(1),\text{exact}}}{dt\, du} = \frac{\alpha_w\, \alpha_s^3}{16\,\pi} \frac{1}{s\,t\,u} \frac{m_H^8}{M_W^2} \frac{N}{N^2 - 1} \left[|A_2(s,t,u)|^2 + |A_2(u,s,t)|^2 \right.$$

$$\left. + |A_2(t,u,s)|^2 + |A_4(s,t,u)|^2 \right] \delta(s + t + u - m_H^2)\,, \qquad (2.4)$$

with

$$\alpha_w = \frac{e^2}{4\pi\, \sin^2 \theta_W} = \frac{\sqrt{2}\, M_W^2\, G_F}{\pi}\,, \qquad (2.5)$$

where e denotes the electric charge and θ_W is the weak angle. The constants M_W and G_F denote the mass of the W and the Fermi constant respectively. Further we want to mention that $N = 3$ for QCD. The dimensionless functions $A_2(s,t,u)$ and $A_4(s,t,u)$ are given in the Appendix of [4]. The Born cross section for the $q + \bar{q} \to g + H$ subprocess in Fig. 2 equals

$$s^2 \frac{d^2 \sigma_{q\bar{q} \to g\ H}^{(1),\text{exact}}}{dt\, du} = \frac{\alpha_w\, \alpha_s^3}{128\,\pi} \frac{u^2 + t^2}{s\,(u + t)^2} \frac{m_H^4}{M_W^2} \frac{N^2 - 1}{N^2} |A_5(s,t,u)|^2$$
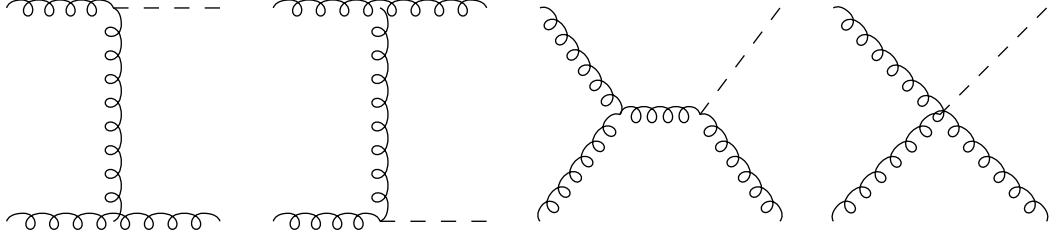
$$\times \delta(s + t + u - m_H^2)\,, \qquad (2.6)$$

Figure 3: The approximate process $g + g \to g + H$.

where the function $A_5(s, t, u)$ is given in the Appendix of [4]. Finally the Born cross section for the $q(\bar{q}) + g \to q(\bar{q}) + H$ reaction becomes (see Fig. 2)

$$s^2 \frac{d^2 \sigma_{qg \to q\ H}^{(1),\text{exact}}}{dt\ du} = -\frac{\alpha_w \alpha_s^3}{128 \pi} \frac{u^2 + s^2}{t(u+s)^2} \frac{m_H^4}{M_W^2} \frac{1}{N} |A_5(t, s, u)|^2$$

$$\times \delta(s + t + u - m_H^2). \tag{2.7}$$

In the limit of infinite top mass m_t the functions above simplify enormously. Actually they can be derived from the effective Lagrangian

$$\mathcal{L}_{eff} = G\,\Phi(x)\,O(x), \quad \text{with} \quad O(x) = -\frac{1}{4}\,G_{\mu\nu}^a(x)\,G^{a,\mu\nu}(x), \tag{2.8}$$

where $\Phi(x)$ represents the Higgs field and G is an effective coupling constant given by

$$G^2 = \frac{\alpha_w \alpha_s^2}{9\pi M_W^2}\,\mathcal{C}^2\left(\alpha_s, \frac{\mu_r^2}{m_t^2}\right). \tag{2.9}$$

The quantity $\mathcal{C}$ is the coefficient function which describes all QCD corrections to the top-quark loops in the limit $m_t \to \infty$. For external gluons, which are on-shell, the latter quantity has been computed up to order α_s in [8], [9], [23] and up to α_s^2 in [24], [25]. Up to second order it reads

$$\mathcal{C}\left(\alpha_s(\mu_r^2), \frac{\mu_r^2}{m_t^2}\right) = 1 + \frac{\alpha_s^{(5)}(\mu_r^2)}{4\pi}\,(11) + \left(\frac{\alpha_s^{(5)}(\mu_r^2)}{4\pi}\right)^2 \left[\frac{2777}{18} + 19\ln\frac{\mu_r^2}{m_t^2}\right.$$

Figure 4: The approximate processes $q + \bar{q} \rightarrow g + H$ and $q(\bar{q}) + g \rightarrow q(\bar{q}) + H$.

$$+n_f \left(-\frac{67}{6} + \frac{16}{3} \ln \frac{\mu_r^2}{m_t^2} \right) \right] . \tag{2.10}$$

Here μ_r represents the renormalization scale and n_f denotes the number of light flavours. Moreover $\alpha_s^{(5)}$ is presented in a five-flavour-number scheme. In the infinite top-quark mass limit the Feynman rules can be derived from Eq. (2.8). In that limit the Born cross sections become

$$s^2 \frac{d^2 \sigma_{gg \rightarrow g \; H}^{(1), m_t \rightarrow \infty}}{dt \; du} = \frac{\alpha_w \, \alpha_s^3}{144 \, \pi} \frac{N}{N^2 - 1} \frac{1}{s \, t \, u \, M_W^2} \left[s^4 + t^4 + u^4 + m_H^8 \right]$$

$$\times \delta(s + t + u - m_H^2) , \tag{2.11}$$

$$s^2 \frac{d^2 \sigma_{q\bar{q} \rightarrow g \; H}^{(1), m_t \rightarrow \infty}}{dt \; du} = \frac{\alpha_w \, \alpha_s^3}{288 \, \pi} \frac{N^2 - 1}{N^2} \frac{t^2 + u^2}{s \, M_W^2} \delta(s + t + u - m_H^2) , \tag{2.12}$$

$$s^2 \frac{d^2 \sigma_{qg \rightarrow q \; H}^{(1), m_t \rightarrow \infty}}{dt \; du} = -\frac{\alpha_w \, \alpha_s^3}{288 \, \pi} \frac{1}{N} \frac{u^2 + s^2}{t \, M_W^2} \delta(s + t + u - m_H^2) , \tag{2.13}$$

where the the graphs are shown in Fig. 3 and 4. The next order gluonic corrections to the $2 \rightarrow 2$ reactions in Figs. 1 and 2 have not been calculated yet. Some of the graphs are shown in Fig. 5, which shows that the calculation will be very tedious. However we can make an approximation. In the infinite top-quark mass limit the soft-plus-virtual $(S + V)$ cross sections could be written as [14]
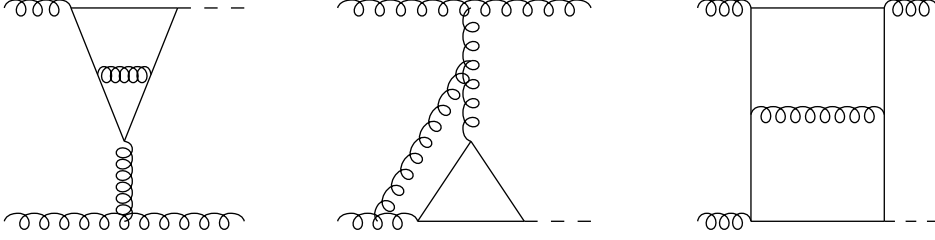
Figure 5: Samples of two-loop graphs contributing to $g + g \rightarrow g + H$.

$$s^2 \frac{d^2 \, \sigma_{ab \rightarrow c\,H}^{(2),\text{S+V}}}{dt \, du} \quad = \quad \frac{\alpha_s}{4\pi} \, N(s,t,u,\Delta,\mu^2) \, s^2 \, \frac{d^2 \, \sigma_{ab \rightarrow c\,H}^{(1)}}{dt \, du}$$

$$+ \pi \, \delta(s+t+u-m_H^2) \frac{\alpha_s}{4\pi} \, K \, |MB_{ab \rightarrow c\,H}^{(1)}|^2 \,. \quad (2.14)$$

Here $d^2\sigma^{(1)}$ denote the Born cross sections in Eqs. (2.11)-(2.13) and $MB_{ab \rightarrow c\,H}^{(1)}$ is a left over piece which is numerically very small. The term $N(s,t,u,\Delta,\mu^2)$ is an universal function which depends on the parameter Δ which serves as a momentum cut off for the infrared divergence. Finally K denotes a combination of colour factors which vanishes in the supersymmetric limit $C_A = C_F = n_f = N$. Here C_A, C_F are the standard colour factors in $SU(N)$. For more details see Eqs. (5.24)-(5.26) in [14]. Since $N(s,t,u,\Delta,\mu^2)$ is universal we replace the Born cross sections in the first term of Eq. (2.14) by the exact ones in Eqs. (2.4), (2.6), (2.7). In this way we get a better soft-plus-virtual gluon approximation for the Higgs boson cross section which is also valid for Higgs masses and transverse momenta p_t larger than the top-quark mass m_t. The $2 \rightarrow 3$ reactions are denoted by

$$a(p_1) + b(p_2) \rightarrow c(p_3) + d(p_4) + H(q) \,,$$

$$s = (p_1 + p_2)^2 \,, \quad t = (p_1 - q)^2 \,, \quad u = (p_2 - q)^2 \,, \quad s_4 = (p_3 + p_4)^2 \,,$$

$$s_4 = s + t + u - m_H^2 \,. \quad (2.15)$$

The matrix elements for the $2 \rightarrow 3$ processes have been exactly calculated in [22] although in four dimensions. Some of the graphs are shown in Fig.
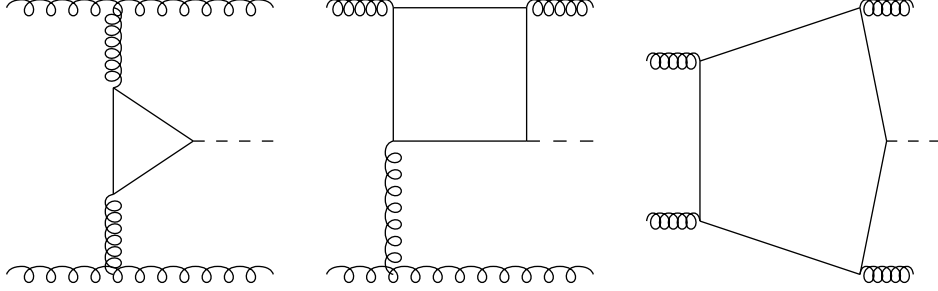
Figure 6: Samples of graphs contributing to $g + g \rightarrow g + g + H$.

6. However we need them in n dimensions to regularize the infrared and collinear divergences (for $n = 4$ there is a problem see [26]). Furthermore we also need the exact virtual corrections to cancel the infrared divergences. Since the latter are not calculated yet we can only make an approximation for the soft parts ($s_4 \rightarrow 0$) of the $2 \rightarrow 3$ processes. In the $m_t \rightarrow \infty$ limit these parts are

$$s^2 \frac{d^2 \sigma_{ab \rightarrow cd\,H}^{(2),\text{SOFT}}}{dt\,du} = \frac{\alpha_s}{4\pi} \frac{1}{s_4} I(s, t, u, s_4, \mu^2) \, s^2 \frac{d^2 \sigma_{ab \rightarrow c\,H}^{(1)}}{dt\,du}, \qquad (2.16)$$

where $d^2\sigma^{(1)}$ are the Born cross sections in the limit $m_t \rightarrow \infty$ given in Eqs. (2.11)-(2.13). The term $I(s, t, u, s_4, \mu^2)$ is a universal factor and contains simple functions which are proportional to $\ln s_4/\mu^2$. For more details see Eqs. (5.16)-(5.20) in [14]. We get a better approximation to the exact cross sections if we replace in Eq. (2.16) the cross sections in $m_t \rightarrow \infty$ limit by the exact ones in Eqs. (2.4), (2.6),(2.7). The most optimal next-to-leading order (NLO) cross section that one can achieve is to use the exact lowest order cross sections in Eq. (2.4), (2.6), (2.7) and in next order to substitute them in Eq. (2.14) and (2.16). This relies upon the fact that the soft-plus-virtual gluon approximation is a very good substitute for the exact cross section. We know from our experience with the cross section in the infinite top-quark mass limit that this is really the case. This is revealed by a study of the transverse momentum p_t and the rapidity y distributions in Figs. 13-15 of [14]. Above $p_t = 100$ GeV/c and $m_H \geq 100$ GeV/c^2 the soft-plus-virtual

gluon approximation accounts for 80 % of the cross section. However we can do even better. This becomes clear if we look at the transverse momentum distribution

$$\frac{d\,\sigma^{H_1 H_2}}{d\,p_t}(S, p_t^2, m_H^2) = \sum_{a,b=q,g} \int_{x_{\min}}^{x_{\max}} dx\, \tilde{\Phi}_{ab}^{H_1 H_2}(x, \mu^2)\, \frac{d\,\sigma_{ab}}{d\,p_t}(xS, p_t^2, m_H^2, \mu^2)\,,$$

(2.17)

with

$$x_{\min} = \frac{m_H^2 + 2\,p_t^2 + 2\,\sqrt{p_t^2\,(p_t^2 + m_H^2)}}{S}\,, \qquad x_{\max} = 1\,, \qquad (2.18)$$

and $\tilde{\Phi}_{ab}$ denotes the momentum fraction luminosity defined by

$$\tilde{\Phi}_{ab}^{H_1 H_2}(x, \mu^2) = \int_0^1 dx_1 \int_0^1 dx_2\, \delta(x - x_1\,x_2)\, f_a^{H_1}(x_1, \mu^2)\, f_b^{H_2}(x_2, \mu^2)\,. \quad (2.19)$$

However Eq. (2.17) can also be cast in the form (see [27])

$$\frac{d\,\sigma^{H_1 H_2}}{d\,p_t}(S, p_t^2, m_H^2) = \sum_{a,b=q,g} x_{\min} \int_{x_{\min}}^{x_{\max}} dx\, \Phi_{ab}^{H_1 H_2}(x, \mu^2)\, \frac{x}{x_{\min}}$$

$$\times \frac{d\,\sigma_{ab}}{d\,p_t}(x\,S, p_t^2, m_H^2, \mu^2)\,,$$

(2.20)

where Φ_{ab} is the parton luminosity given by

$$\Phi_{ab}^{H_1 H_2}(x, \mu^2) = x^{-1}\,\tilde{\Phi}_{ab}^{H_1 H_2}(x, \mu^2)\,. \qquad (2.21)$$

If we consider the whole cross section it makes no difference which definition we are using. However if we limit ourselves to the soft-plus-virtual gluon approximation and moreover we set $x/x_{\min} = 1$ in Eq. (2.20) we get a difference. In fact we enhance the small x region which leads to an improvement of the approximation. This is mainly due to the fact that the small x gluons dominate the differential distributions as they already did in the total cross section (see [11]-[14]). This will be shown in the next section.

3 Differential distributions for the LHC and the TEVATRON

In this section the hadronic differential distributions are presented for arbitrary Higgs mass m_H and top-quark mass m_t. We compare the results for the NLO differential cross sections in the infinite top-quark mass limit and in the approximation derived in the previous section, which is valid for arbitrary m_t. Since the latter is only defined for the transverse momentum we will limit ourselves to the p_t-distributions. In this paper we will study Higgs boson production in proton-proton collisions at LHC ($\sqrt{S} = 14.0$ TeV) and proton-anti-proton collisions at the TEVATRON ($\sqrt{S} = 2.0$ TeV). The hadronic cross section is obtained from the partonic cross section as follows

$$S^2 \frac{d^2 \, \sigma^{\mathrm{H_1 H_2}}}{d \, T \, d \, U}(S,T,U,m_H^2) \;\; = \;\; \sum_{a,b=q,g} \int_{x_{1,\mathrm{min}}}^1 \frac{dx_1}{x_1} \int_{x_{2,\mathrm{min}}}^1 \frac{dx_2}{x_2} \, f_a^{\mathrm{H_1}}(x_1,\mu^2)$$

$$\times f_b^{\mathrm{H_2}}(x_2,\mu^2) \, s^2 \frac{d^2 \, \sigma_{ab}}{d \, t \, d \, u}(s,t,u,m_H^2,\mu^2) \, . \tag{3.1}$$

In analogy to Eq. (2.2) the hadronic kinematical variables are defined by

$$S = (P_1 + P_2)^2 \, , \qquad T = (P_1 - q)^2 \, , \qquad U = (P_2 - q)^2 \, , \tag{3.2}$$

where P_1 and P_2 denote the momenta of hadrons H_1 and H_2 respectively (see Eq. (2.1)). In the case parton p_1 emerges from hadron $H_1(P_1)$ and parton p_2 emerges from hadron $H_2(P_2)$ we can establish the following relations

$$p_1 = x_1 \, P_1 \, , \qquad p_2 = x_2 \, P_2 \, ,$$

$$s = x_1 \, x_2 \, S \, , \quad t = x_1(T - m_H^2) + m_H^2 \, , \quad u = x_2(U - m_H^2) + m_H^2 \, ,$$

$$x_{1,\mathrm{min}} = \frac{-U}{S + T - m_H^2} \, , \qquad x_{2,\mathrm{min}} = \frac{-x_1(T - m_H^2) - m_H^2}{x_1 S + U - m_H^2} \, . \tag{3.3}$$

From Eq. (3.1) one can obtain the p_t and y distributions. Neglecting the masses of the incoming hadrons we have the following relations

$$T = m_H^2 - \sqrt{S} \, \sqrt{p_t^2 + m_H^2} \, \cosh y + \sqrt{S} \, \sqrt{p_t^2 + m_H^2} \, \sinh y \, ,$$

$$U = m_H^2 - \sqrt{S}\,\sqrt{p_t^2 + m_H^2}\,\cosh y - \sqrt{S}\,\sqrt{p_t^2 + m_H^2}\,\sinh y\,, \quad (3.4)$$

so that the cross section becomes

$$S\frac{d^2\,\sigma^{\mathrm{H_1H_2}}}{d\,p_t^2\,d\,y}(S, p_t^2, y, m_H^2) = S^2\frac{d^2\,\sigma^{\mathrm{H_1H_2}}}{d\,T\,d\,U}(S, T, U, m_H^2)\,. \quad (3.5)$$

The kinematical boundaries are

$$m_H^2 - S \leq T \leq 0\,, \qquad -S - T + m_H^2 \leq U \leq \frac{S\,m_H^2}{T - m_H^2} + m_H^2\,, \quad (3.6)$$

from which one can derive

$$0 \leq p_t^2 \leq p_{t,\mathrm{max}}^2\,, \qquad -\frac{1}{2}\ln\frac{S}{m_H^2} \leq y \leq \frac{1}{2}\ln\frac{S}{m_H^2}\,,$$

$$\text{with}\quad p_{t,\mathrm{max}}^2 = \frac{(S + m_H^2)^2}{4\,S\,\cosh^2 y} - m_H^2\,, \quad (3.7)$$

or

$$-y_{\mathrm{max}} \leq y \leq y_{\mathrm{max}}\,, \qquad 0 \leq p_t^2 \leq \frac{(S - m_H^2)^2}{4\,S} \equiv p_{T,\mathrm{max}}^2\,,$$

$$\text{with}\quad y_{\mathrm{max}} = \frac{1}{2}\ln\frac{1 + \sqrt{1 - sq}}{1 - \sqrt{1 - sq}}\,, \qquad sq = \frac{4\,S\,(p_t^2 + m_H^2)}{(S + m_H^2)^2}\,. \quad (3.8)$$

We can perform the integral over the rapidity and obtain the transverse momentum distribution

$$\frac{d\,\sigma^{\mathrm{H_1H_2}}}{d\,p_t}(S, p_t^2, m_H^2) = \int_{-y_{\mathrm{max}}}^{y_{\mathrm{max}}} dy\,\frac{d^2\,\sigma^{\mathrm{H_1H_2}}}{d\,p_t\,d\,y}(S, p_t^2, y, m_H^2)\,, \quad (3.9)$$

with y_{max} given in Eq. (3.8). An alternative way to obtain the distribution above is given in Eq. (2.17). We checked that both procedures lead to the same numerical result.

We define what we mean by leading order (LO) and next-to-leading order (NLO). In the infinite top-quark mass limit and in the exact computation the differential cross section in LO is defined by

$$\frac{d\,\sigma^{\mathrm{LO}}}{d\,p_t}(S, p_t^2, m_H^2) = \frac{d\,\sigma^{(1)}}{d\,p_t}(S, p_t^2, m_H^2)\,, \quad (3.10)$$

where we shall denote the LO cross section in the infinite top-quark mass limit by $d\sigma^{\mathrm{LO},m_t\to\infty}/dp_t$. The partonic cross sections in the latter quantity are given in Eqs. (2.11)-(2.13). The exact LO cross section is represented by $d\sigma^{\mathrm{LO,exact}}/dp_t$ with the partonic cross sections in Eqs. (2.4), (2.6) and (2.7). The gluon-gluon-Higgs coupling is given by G in Eq. (2.9) with $\mathcal{C}=1$. The top-quark mass is given by $m_t = 174.3$ GeV/c^2 and the Fermi constant $G_F = 1.16639 \times 10^{-5}\,\mathrm{GeV}^{-2} = 4541.68$ pb in Eq. (2.5). We also adopt the leading logarithmic representation for the running coupling and the parton densities. For the latter we choose the parametrization according to [28] (namely set lo2002.dat) with $\Lambda_5^{\mathrm{LO}} = 167$ MeV and $n_f = 5$.

The NLO corrected differential cross section in the asymptotic top-quark mass limit is given by

$$
\frac{d\,\sigma^{\mathrm{NLO},m_t\to\infty}}{d\,p_t}(S, p_t^2, m_H^2) = \left[1 + 22\left(\frac{\alpha_s^{(5)}(\mu^2)}{4\pi}\right)\right]\frac{d\,\sigma^{\mathrm{LO},m_t\to\infty}}{d\,p_t}(S, p_t^2, m_H^2)
$$

$$
+\frac{d\,\sigma^{(2),m_t\to\infty}}{d\,p_t}(S, p_t^2, m_H^2)\,, \tag{3.11}
$$

In $d\,\sigma^{(2),m_t\to\infty}$ all partonic cross sections use the asymptotic top-quark mass limit results in [15]-[18]. Further we have multiplied the LO cross section by $\mathcal{C}^2 = 1 + 22\,\alpha_s/4\pi$ in Eq. (2.10). Finally we have the approximation for arbitrary masses m_H and m_t

$$
\frac{d\,\sigma^{\mathrm{NLO,approx}}}{d\,p_t}(S, p_t^2, m_H^2) = \frac{d\,\sigma^{\mathrm{LO,exact}}}{d\,p_t}(S, p_t^2, m_H^2)
$$

$$
+\frac{d\,\sigma^{\mathrm{S+V,approx}}}{d\,p_t}(S, p_t^2, m_H^2)\,, \tag{3.12}
$$

where the partonic cross sections are given in Eqs. (2.4), (2.6) and (2.7) and the soft-plus-virtual gluon approximation is given in Eqs. (2.14) and (2.16). The running coupling and parton densities are also represented in next-to-leading order for which we have chosen the $\overline{\mathrm{MS}}$-scheme and $n_f = 5$. For our plots we have adopted the parametrization obtained from the set MRST [29] (namely set alf119.dat) with $\Lambda_5^{\mathrm{NLO}} = 239$ MeV. For simplicity the factorization scale μ is set equal to the renormalization scale μ_r. For our plots we take $\mu = \mu_0 = \sqrt{p_t^2 + m_H^2}$ unless mentioned otherwise.

Our first study concerns the validity of the soft-plus-virtual gluon approximation. This is done in the asymptotic top-quark limit where we know the complete NLO correction. For that purpose we plot

$$R = \frac{d\sigma^{\text{S+V},m_t\to\infty}/dp_t}{d\sigma^{\text{NLO},m_t\to\infty}/dp_t} \qquad (3.13)$$

in the range $40\,\text{GeV/c} < p_t < 200\,\text{GeV/c}$ and $m_H = 120,\ 160,\ 200\,\text{GeV/c}^2$. The plots are given for the LHC ($\sqrt{S} = 14$ GeV) in Fig. 7. The figure reveals that at $m_H = 120\,\text{GeV/c}^2$ and $p_t = 40\,\text{GeV/c}$ the ratio is 1.06 and it decreases to about 0.9 at $p_t = 200\,\text{GeV/c}$. For larger Higgs masses the ratio becomes closer to unity at $p_t > 100$ GeV/c. This feature can be understood because at larger Higgs masses the kinematics are closer to the boundary of phase space. The conclusion is that in the range $100\,\text{GeV/c} < p_t < 200\,\text{GeV/c}$ we have $0.9 < R < 1.0$ which indicates that the soft-plus-virtual gluon approximation with the prescription in [27] works rather well. This is mainly due to the dominance of the gg-channel and the steeply rising gluon flux which is even enhanced by the definition of the parton luminosity in Eqs. (2.20), (2.21). In the case of the TEVATRON ($\sqrt{S} = 2$ GeV) the soft-plus-virtual gluon approximation works even better (see Fig. 8). In the whole range $40\,\text{GeV/c} < p_t < 200\,\text{GeV/c}$ we have $0.95 < R < 1.07$. However the mass range is more limited i.e. $m_H = 120,\ 130,\ 140\,\text{GeV/c}^2$ because at larger masses the cross section becomes unobservably small. This is understandable because at lower energies we are closer to the boundary of phase space where the soft-plus-virtual gluon approximation approaches the exact cross section. The transverse momentum distributions $d\,\sigma/d\,p_t$ are plotted in the case of the LHC in Figs. 9, 10, 11 for $m_H = 120,\ 160,\ 200\,\text{GeV/c}^2$ respectively. The figures reveal the differences between the cross sections in the asymptotic m_t limits and the exact (approximate) cross sections. They becomes more clear if we plot the ratios

$$H^{\text{LO}} = \frac{d\sigma^{\text{LO,exact}}/dp_t}{d\sigma^{\text{LO},m_t\to\infty}/dp_t}, \qquad H^{\text{NLO}} = \frac{d\sigma^{\text{NLO,approx}}/dp_t}{d\sigma^{\text{NLO},m_t\to\infty}/dp_t}, \qquad (3.14)$$

which are shown in Figs. 12, 13 and 14. For the Born cross section they vary at $p_t = 40$ GeV/c from 0.93 to 1.03 for $m_H = 120\,\text{GeV/c}^2$ to $200\,\text{GeV/c}^2$ respectively. At $p_t = 200$ GeV/c they all become about 0.8 irrespective of the Higgs mass. For the NLO cases these values are 0.96 to 1.28 for small

p_t and 0.68 to 0.75 at large p_t as m_H increases from $m_H = 120$ GeV/c^2 to $m_H = 200$ GeV/c^2. The exact (approximate) cross sections are always below those in the asymptotic m_t limit except for $m_H = 160$ GeV/c^2 and $m_H = 200$ GeV/c^2 at small p_t. There are cross over points at $p_t = 55$ GeV/c and $p_t = 75$ GeV/c for the NLO cross sections. The NLO corrections are very large. This becomes clear if we look at the K-factors defined by

$$K = \frac{d\,\sigma^{\mathrm{NLO,approx}}/d\,p_t}{d\,\sigma^{\mathrm{LO,exact}}/d\,p_t},\tag{3.15}$$

which are shown in Fig. 15. At $p_t = 40$ GeV/c the K-factors vary from 1.66 to 2.02 as m_H increases from $m_H = 120$ GeV/c^2 to $m_H = 200$ GeV/c^2 respectively. At larger p_t values the K-factors decrease and at $p_t = 120$ GeV/c they stabilise around the values 1.5, 1.55, 1.65 for $m_H = 120, 160, 200$ GeV/c^2 respectively. For $m_H = 120$ GeV/c^2 the difference between the asymptotic m_t limit and the soft-plus-virtual gluon approximation in NLO is of the same order as the K-factors, namely 1.5. In Fig. 16 the transverse momentum distributions are shown for the TEVATRON at $m_H = 120$ GeV/c^2 and in Fig. 17 the ratios in Eq. (3.14) are plotted. Here the discrepancies in NLO are even larger. There is very little difference between small p_t and large p_t and the approximate cross section is about 0.5 to 0.8 times smaller than the one in the asymptotic m_t limit. The Born approximations vary from 0.8 to 1.25 when p_t ranges from $p_t = 40$ GeV/c to $p_t = 200$ GeV/c. Notice that for $p_t > 135$ GeV/c the approximate cross section becomes even a little bit larger than the one in the case of the asymptotic m_t limit. The K-factors (see Fig. 18) are a little bit smaller than in the case of the LHC. At $p_t = 40$ GeV/c they vary between 1.5 and 1.8 and at larger p_t (say $p_t > 120$ GeV/c) they are in the range $1.3 < K < 1.4$. Here the discrepancy between the asymptotic m_t limit and the approximate cross section in NLO is even larger than the corresponding K-factor. Note that the peaks in Figs. 16 and 17 reflect the thresholds in the partonic channels described in [3]-[7]. The dependence of the exact Born and the soft-plus-virtual gluon approximation cross sections on the factorization scale μ is studied for $m_H = 120$ GeV/c^2 at $p_t = 100, 150, 200$ GeV/c. The dependence can be expressed by the following quantity

$$N\left(p_t, \frac{\mu}{\mu_0}\right) = \frac{d\sigma^{\mathrm{approx}}(p_t, \mu)/dp_t}{d\sigma^{\mathrm{approx}}(p_t, \mu_0)/dp_t}\tag{3.16}$$

with $\mu_0 = \sqrt{p_t^2 + m_H^2}$. This quantity is plotted in the range $0.1\ \mu_0 < \mu < 10\ \mu_0$ for LO and NLO in Fig. 19 for the LHC and in Fig. 20 for the TEVATRON both at $m_H = 120$ GeV/c^2. The LO cross sections have the larger values for small μ/μ_0. What is very striking is the improvement in scale variation while going from LO to NLO. In LO there is steep behaviour at small μ/μ_0 which is flattened out in NLO. At large μ/μ_0 the difference between LO and NLO is not so big, but still the NLO curves are flatter than the LO ones. Basically the same curves are also found at larger Higgs masses so that there is no need to show them. Finally there is a small dependence of $N(p_t, \mu/\mu_0)$ on the transverse momenta in both LO and in NLO.

Concluding our findings we observe that the soft-plus-virtual gluon approximation gives a good description of the exact NLO cross section (within 90 %), when tested with $m_t \rightarrow \infty$ cross sections. The difference between the asymptotic m_t limit and the soft-plus-virtual gluon approximation is larger than the K-factor in the case of the TEVATRON but smaller than the K-factor in the case of the LHC. Also the validity of asymptotic m_t limit depends more on the value of the transverse momentum than on the magnitude of the Higgs mass. Finally our approximation has a significantly smaller scale dependence for both colliders in particular at small factorization scale.

References

[1] J.F. Gunion, H.E. Haber, G.L. Kane, S. Dawson, "The Higgs Hunter's Guide", (Addison-Wesley, Reading, M.A.,1990), Erratum ibid. hep/ph-9302272.

[2] F. Wilczek, Phys. Rev. Lett. 39 (1977) 1304;
H. Georgi, S. Glashow, M. Machacek, D. Nanopoulos, Phys. Rev. Lett, 40 (1978) 692;
J. Ellis, M. Gaillard, D. Nanopoulos, C. Sachrajda, Phys. Lett. B83 (1979) 339;
T. Rizzo, Phys. Rev. D22 (1980) 178.

[3] I. Hinchliffe, S.F. Novaes, Phys. Rev. D38 (1988) 3475.

[4] R.K. Ellis, I. Hinchliffe, M. Soldate, J.J. van der Bij, Nucl. Phys. B297 (1988) 221.

[5] U. Baur, E. Glover, Nucl. Phys. B339 (1990) 38.

[6] R.P. Kauffman, Phys. Rev. D44 (1991) 1415, ibid. D45 (1992) 1512.

[7] B. Field, S. Dawson, J. Smith, Phys. Rev. D69 (2004) 074013, hep-ph/0311199.

[8] D. Graudenz, M. Spira, P. Zerwas, Phys. Rev. Lett. 70 (1993) 1372;
M. Spira, A. Djouadi, D. Graudenz, P. Zerwas, Nucl. Phys. B453 (1995) 17, hep-ph/9504378.

[9] S. Dawson, Nucl. Phys. B359 (1991) 283;
A. Djouadi, M. Spira, P. Zerwas, Phys. Lett. B264 (1991) 440.

[10] R.V. Harlander, Phys. Lett. B492 (2000) 74, hep-ph/0007289;
V. Ravindran, J. Smith, W.L. van Neerven, Nucl. Phys. B704 (2005) 332, hep-ph/0408315, ibid. Nucl. Phys. B(Proc. Suppl) 135 (2004) 35, hep-ph/0405263.

[11] S. Catani, D. de Florian, M. Grazzini, JHEP 0105 (2001) 025, hep-ph/0102227;
R.V. Harlander, W.B. Kilgore, Phys. Rev. D64 (2001) 013015; hep-ph/0102241.

[12] R.V. Harlander, W.B. Kilgore, Phys. Rev. Lett. 88 (2002) 201801, hep-ph/0201206, ibid. JHEP 0210 (2002) 017, hep-ph/0208096.

[13] C. Anastasiou, K. Melnikov, Nucl. Phys. B646 (2002) 220, hep-ph/0207004, Phys. Rev. D67 (2003) 037501, hep-ph/0208115.

[14] V. Ravindran, J. Smith, W.L. van Neerven, Nucl. Phys. B665 (2003) 325, hep-ph/0302135, ibid. Pramana 62 (2004) 683, hep-ph/0304005.

[15] D. de Florian, M. Grazzini, Z. Kunszt, Phys. Rev. Lett. 82 (1999) 5209, hep-ph/9902483.

[16] V. Ravindran, J. Smith, W.L. van Neerven, Nucl. Phys. B634 (2002) 247, hep-ph/0201114.

[17] C.J. Glosser, C.J. Schmidt, JHEP 0212 (2002) 016, hep-ph/0209248.

[18] B. Field, J. Smith, M.E. Tejeda-Yeomans, W.L. van Neerven, Phys. Lett. B551 (2003) 137, hep-ph/0210369.

[19] G. Bozzi, S. Catani, D. de Florian, M. Grazzini, Phys. Lett. B564 (2003) 65, hep-ph/0302104.

[20] A. Kulesza, G. Sterman, W. Vogelsang, Phys. Rev. D69 (2004) 014012, hep-ph/0309264.

[21] B. Field, Phys. Rev. D70 (2004) 054008, hep-ph/0405219.

[22] V. Del Duca, W. Kilgore, C. Oleari, C. Schmidt, D. Zeppenfeld, Phys. Rev. Lett. 87 (2001) 122001, hep-ph/0105129, ibid. Nucl. Phys. B616 (2001) 367, hep-ph/0108030.

[23] S. Dawson, R.P. Kauffman, Phys. Rev. Lett. 68 (1992) 2273.

[24] K.G. Chetyrkin, B.A. Kniehl, M. Steinhauser, Phys. Rev. Lett. 79 (1997) 353, hep-ph/9705240.

[25] M. Krämer, E. Laenen, M. Spira, Nucl. Phys. B511 (1998) 523, hep-ph/9611272.

[26] J. Smith, W.L. van Neerven, hep-ph/0411357.

[27] S. Catani, D. de Florian, M. Grazzini, JHEP 0201 (2002) 015, hep-ph/0111164.

[28] A.D. Martin, R.G. Roberts, W.J. Stirling, R.S. Thorne, Phys. Lett. B531 (2002) 216, hep-ph/0201127.

[29] A.D. Martin, R.G. Roberts, W.J. Stirling, R.S. Thorne, Eur. Phys. J. C23 (2002) 73, hep-ph/0110215.

Figure Captions

Fig. 7. The quality of the soft-plus-virtual gluon approximation represented by the ratio R in Eq. (3.13) for $40\,\mathrm{GeV/c} < p_t < 200\,\mathrm{GeV/c}$ at the LHC ($\sqrt{S} = 14$ TeV) for $m_H = 120\,\mathrm{GeV/c^2}$ (solid line), $m_H = 160\,\mathrm{GeV/c^2}$ (dashed line), $m_H = 200\,\mathrm{GeV/c^2}$ (dotted line).

Fig. 8. The quality of the soft-plus-virtual gluon approximation represented by the ratio R in Eq. (3.13) for $40\,\mathrm{GeV/c} < p_t < 200\,\mathrm{GeV/c}$ at the TEVATRON ($\sqrt{S} = 2$ TeV) for $m_H = 120\,\mathrm{GeV/c^2}$ (solid line), $m_H = 130\,\mathrm{GeV/c^2}$ (dashed line), $m_H = 140\,\mathrm{GeV/c^2}$ (dotted line).

Fig. 9. Differential cross sections at the LHC ($\sqrt{S} = 14$ TeV) with $m_H = 120\,\mathrm{GeV/c^2}$. The Born cross sections $d\sigma^{\mathrm{LO,exact}}/dp_t$ (dotted line) and $d\sigma^{\mathrm{LO,m_t\to\infty}}/dp_t$ (dot-dashed line). Also shown are the NLO contributions $d\sigma^{\mathrm{NLO,approx}}/dp_t$ (solid line) and $d\sigma^{\mathrm{NLO,m_t\to\infty}}/dp_t$ (dashed line).

Fig. 10. Differential cross sections at the LHC ($\sqrt{S} = 14$ TeV) with $m_H = 160\,\mathrm{GeV/c^2}$. The Born cross sections $d\sigma^{\mathrm{LO,exact}}/dp_t$ (dotted line) and $d\sigma^{\mathrm{LO,m_t\to\infty}}/dp_t$ (dot-dashed line). Also shown are the NLO contributions $d\sigma^{\mathrm{NLO,approx}}/dp_t$ (solid line) and $d\sigma^{\mathrm{NLO,m_t\to\infty}}/dp_t$ (dashed line).

Fig. 11. Differential cross sections at the LHC ($\sqrt{S} = 14$ TeV) with $m_H = 200\,\mathrm{GeV/c^2}$. The Born cross sections $d\sigma^{\mathrm{LO,exact}}/dp_t$ (dotted line) and $d\sigma^{\mathrm{LO,m_t\to\infty}}/dp_t$ (dot-dashed line). Also shown are the NLO contributions $d\sigma^{\mathrm{NLO,approx}}/dp_t$ (solid line) and $d\sigma^{\mathrm{NLO,m_t\to\infty}}/dp_t$ (dashed line).

Fig. 12. The factors H^{LO} (dashed line) and H^{NLO} (solid line) in Eq. (3.14) at the LHC ($\sqrt{S} = 14$ TeV) with $m_H = 120\,\mathrm{GeV/c^2}$.

Fig. 13. Same as in Fig. 12 for $m_H = 160\,\mathrm{GeV/c^2}$.

Fig. 14. Same as in Fig. 12 for $m_H = 200\,\mathrm{GeV/c^2}$.

Fig. 15. The K factor (Eq. (3.15)) for the LHC ($\sqrt{S} = 14$ TeV). $m_H = 120\,\mathrm{GeV/c^2}$ (solid line), $m_H = 160\,\mathrm{GeV/c^2}$ (dashed line), $m_H = 200\,\mathrm{GeV/c^2}$ (dotted line).

Fig. 16. Same as in Fig. 9 but then for the TEVATRON ($\sqrt{S} = 2$ TeV) and $m_H = 120\,\mathrm{GeV/c^2}$.

Fig. 17. Same as in Fig. 12 but then for the TEVATRON ($\sqrt{S} = 2$ TeV) and $m_H = 120\,\text{GeV}/\text{c}^2$.

Fig. 18. The K factor (Eq. (3.15)) for the TEVATRON ($\sqrt{S} = 2$ TeV). $m_H = 120\,\text{GeV}/\text{c}^2$ (solid line), $m_H = 130\,\text{GeV}/\text{c}^2$ (dashed line), $m_H = 140\,\text{GeV}/\text{c}^2$ (dotted line).

Fig. 19. The scale dependence represented by $N(p_t, \mu/\mu_0)$ in Eq. (3.16) for the LHC ($\sqrt{S} = 14$ TeV) and $m_H = 120\,\text{GeV}/\text{c}^2$. The results are plotted in the range $0.1 < \mu/\mu_0 < 10$ with $\mu_0^2 = m_H^2 + p_t^2$ for $p_t = 100\,\text{GeV}/\text{c}$ (solid line), $p_t = 150\,\text{GeV}/\text{c}$ (dashed line) $p_t = 200\,\text{GeV}/\text{c}$ (dotted line). The upper three curves are for $d\sigma^{\text{LO,exact}}/dp_t$ whereas the lower three curves are for $d\sigma^{\text{NLO,approx}}/dp_t$.

Fig. 20. The scale dependence represented by $N(p_t, \mu/\mu_0)$ in Eq. (3.16) for the TEVATRON ($\sqrt{S} = 2$ TeV) and $m_H = 120\,\text{GeV}/\text{c}^2$. The results are plotted in the range $0.1 < \mu/\mu_0 < 10$ with $\mu_0^2 = m_H^2 + p_t^2$ for $p_t = 100\,\text{GeV}/\text{c}$ (solid line), $p_t = 150\,\text{GeV}/\text{c}$ (dashed line) $p_t = 200\,\text{GeV}/\text{c}$ (dotted line). The upper three curves are for $d\sigma^{\text{LO,exact}}/dp_t$ whereas the lower three curves are for $d\sigma^{\text{NLO,approx}}/dp_t$.